Effects of ensembles, ligand, and strain on adsorbate binding to alloy surfaces

Hao Li,[a)] Kihyun Shin,[a)] and Graeme Henkelman[b)]
Department of Chemistry and the Institute for Computational Engineering and Sciences,
The University of Texas at Austin, 105 E. 24th Street, Stop A5300, Austin, Texas 78712, USA

Alloying elements with strong and weak adsorption properties can produce a catalyst with optimally tuned adsorbate binding. A full understanding of this alloying effect, however, is not well-established. Here, we use density functional theory to study the ensemble, ligand, and strain effects of close-packed surfaces alloyed by transition metals with a combination of strong and weak adsorption of H and O. Specifically, we consider PdAu, RhAu, and PtAu bimetallics as ordered and randomly alloyed (111) surfaces, as well as randomly alloyed 140-atom clusters. In these alloys, Au is the weak-binding component and Pd, Rh, and Pt are characteristic strong-binding metals. In order to separate the different effects of alloying on binding, we calculate the tunability of H- and O-binding energies as a function of lattice constant (strain effect), number of alloy-substituted sublayers (ligand effect), and randomly alloyed geometries (ensemble effect). We find that on these alloyed surfaces, the ensemble effect more significantly tunes the adsorbate binding as compared to the ligand and strain effects, with the binding energies predominantly determined by the local adsorption environment provided by the specific triatomic ensemble on the (111) surface. However, we also find that tuning of adsorbate binding from the ligand and strain effects cannot be neglected in a quantitative description. Extending our studies to other bimetallics (PdAg, RhAg, PtAg, PdCu, RhCu, and PtCu), we find similar conclusions that the tunability of adsorbate binding on random alloys is predominately described by the ensemble effect. *Published by AIP Publishing.* https://doi.org/10.1063/1.5053894

I. INTRODUCTION

Alloys have been widely studied for heterogeneous catalysis,[1,2] sensor design,[3] and energy storage.[4] Many bi- and multi-metallic alloys exhibit enhanced performance as compared to their monometallic counterparts.[5–9] The origin of the enhanced performance of alloy surfaces has been extensively discussed over the past decade. For alloyed single-crystals or particles with large facets, there are three major effects that are considered to tune alloy surface properties, namely, the ensemble (geometric),[6,10,11] ligand (electronic),[10] and strain effects.[12,13] The ensemble effect describes changes in the local chemisorption properties with a direct change in the atomic ensemble components in the adsorption site,[10] including the binding geometry of adsorbates on the surface. The ligand effect describes the tuning of the surface electronic structure in the same surface ensemble but in a different atomic environment,[10,14] including the electronic contribution from the near-surface to the surface[13] and electronic contributions from the surface atoms around the specific ensemble. The strain effect describes the changes in bond lengths of materials due to differences in the lattice constants of the components, which in turn changes the chemisorption properties.[13] In previous experimental studies on alloy surfaces,

the enhanced performance of alloys has often been attributed to one or two of these effects.[6,8,9,15–17] With an understanding of these effects, new catalysts can be designed, including core@shell catalysts designed by the tuning of adsorbate binding originated from both ligand and strain effects,[18] and random alloys with specific surface compositions to provide highly catalytically active sites due to the ensemble effect.[6]

Experimentally, it is difficult to differentiate these effects on alloy surfaces due to the heterogeneous distribution of atomic ensembles. Although some experimental techniques including temperature-programmed desorption[19] (TPD) can help us to differentiate surface ensembles, the information is limited. For example, it is known that Pd(111) and Au(111), respectively, bind to H strongly and weakly,[20,21] while the PdAu(111) surfaces have a H binding energy intermediate to Pd and Au.[8,17,22] Our previous studies have shown that TPD can differentiate the H_2 desorption peaks from Pd(111)-like and Pd-Au interface sites on PdAu(111) single-crystals,[16,22–26] but TPD cannot differentiate the sizes and geometries of Pd or Pd-Au ensembles due to an overlap of the desorption peaks. However, it was found from density functional theory (DFT) calculations that different sizes and geometries of Pd(111)-like and Pd-Au interface sites have different selectivities and activities for catalytic reactions.[7,16,22,27] Limited characterization of the surface (and subsurface) structure leads to difficulties in identifying the dominant alloying effects. While some advanced atomic-level imaging

---

[a)]H. Li and K. Shin contributed equally to this work.
[b)]Author to whom correspondence should be addressed: henkelman@ utexas.edu

techniques (e.g., scanning tunneling microscope[28]) can elucidate surface ensembles on single-crystals in ultrahigh vacuum, there is currently a lack of *in situ* techniques that can identify active catalytic sites under reaction conditions, leading to uncertainties in mechanistic descriptions of how catalysts function.

To understand alloying effects, DFT has proven as an effective technique to analyze the energy and pathways of catalytic reactions. For heterogeneous catalysis on metallic surfaces, reaction selectivity and activity can be understood from kinetic information calculated by DFT, which in turn can be explained by the binding energies of adsorbates through Brønsted–Evans–Polanyi (BEP) linear relationships between reaction and activation energies[29] and linear scaling relationships between adsorbate binding energies.[30] It has been widely accepted that the tuning of adsorption energies on the alloy surface can be explained by a shift of the electronic *d*-band center due to ligand and strain effects,[12] as well as linear interpolation models to describe ensemble effects.[10] However, it was recently found that although linear interpolation can roughly predict the binding energies of some adsorbates [e.g., O and S on the PdAu(111) surface alloy[10,31]], it fails to explain the binding energies of other species (e.g., H on PtAu, IrAg, and PdRh,[17,32,33] and OH on PtAu, IrAu, PdAg, PtAg, and IrAg[6]) due to different tunability properties of specific surface ensembles. With only a few theoretical studies attempting to distinguish these different effects for a description of adsorption on alloy surfaces,[10,11] we are motivated to disentangle them here.

In this paper, we explore the alloying effects on adsorbate binding energies at close-packed bimetallic surfaces and directly compare the ensemble, ligand, and strain effects. Specifically, we study alloying elements with strong and weak adsorption capacities and explain the resulting changes in the adsorbate binding on these alloyed surfaces.[6,8,9,17] Using PdAu, RhAu, and PtAu as examples, we calculate the H and O binding energies on their (111) surfaces. Ordered and
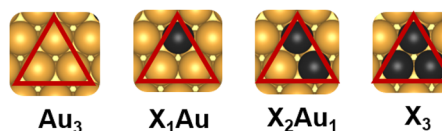

FIG. 1. Three-fold triatomic ensembles considered as binding sites for H and O. The triangles represent the three-fold symmetry of the binding site. The gold and black spheres represent Au and the other alloyed element, respectively.

randomly alloyed slabs as well as randomly alloyed clusters were considered. Additionally, we explore the binding of H and O at other transition metal bimetallics with the random alloy cluster model and discuss the possible interesting effects including the bifunctional effect of Cu-based alloys for catalysis.

II. METHODS

A. Computational methods

All calculations in this study were performed using the VASP code. The generalized gradient approximation method with the Perdew–Burke–Ernzerhof[34] functional was used to describe electronic exchange and correlation. The projector augmented-wave method was used to describe the core electrons.[35] Kohn–Sham wave functions were then expanded in a plane wave basis with an energy cutoff of 400 eV to describe the valence electrons.[36] Geometries were considered relaxed when the forces on each atom decreased below 0.05 eV/Å. For the slab model calculations, a $(3 \times 3 \times 1)$ Monkhorst–Pack *k*-point mesh was used to sample the Brillouin zone.[37] A gamma point sampling was used for the cluster model. Spin polarization was tested and used as needed, such as for the calculation of O_2 in a vacuum.

B. Modeling details

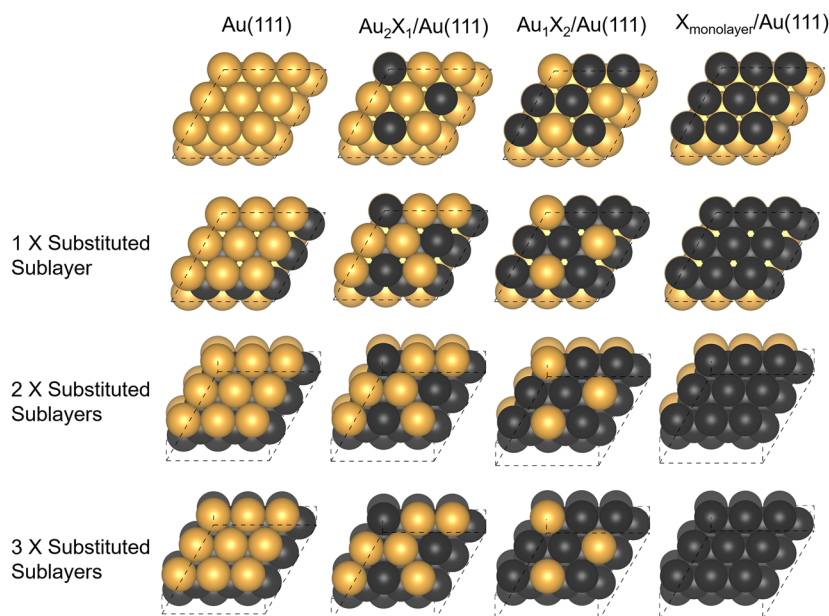In our previous studies, we found that on close-packed surfaces, triatomic ensembles with three-fold symmetry are

FIG. 2. Ordered alloy XAu(111) (X = Pd, Rh, and Pt) surfaces modeled in this study. The gold and black spheres represent Au and the other alloyed element, respectively.

the smallest units for H and O adsorptions (Fig. 1),[6–9,32] which most directly determine the adsorption environment; the atoms outside the triatomic ensemble are less important.[6,8,9,22] Therefore, adsorption is described in terms of the makeup of the triatomic ensemble in this paper. The four triatomic ensembles are denoted as follows: Y_3, X_1Y_2, X_2Y_1, and X_3 (where X and Y represent the two alloy elements, respectively). Examples of the XAu triatomic ensemble are shown in Fig. 1. To find stable adsorption geometries, H and O adsorbates were initially placed at the hollow, bridge, and atop sites of the triatomic ensemble before DFT optimization; after convergence, the optimized site with the favorable binding energy for each specific triatomic ensemble is the one considered in our subsequent analysis.

H- and O-binding energies, E_b, were calculated as

$$E_b = E_{tot} - E_* - \frac{1}{2}E_{gas}, \tag{1}$$

where E_{tot} is the total energy of the system with the adsorbate H or O, E_* is the energy of the bare surface, and E_{gas} is the total energy of H_2 or O_2 in a vacuum.

Ordered alloyed (111) surfaces were modeled as slabs with 4 layers, in p(3 × 3) unit cells, with the bottom two atomic layers fixed in bulk positions. A vacuum gap of at least 12 Å in the z-direction was modeled to separate difference images. The surfaces of the slab were modeled as in Fig. 2: Au(111), X_1Au_2/Au(111), X_2Au_1/Au(111), and $X_{monolayer}$/Au(111). The ordered X_1Au_2/Au(111) and X_2Au_1/Au(111) surfaces contain only the X_1Au_2 and X_2Au_1 ensembles (Fig. 1).[26] To compare and differentiate the ensemble and strain effects, the lattice constant of each surface was tuned between the lattice constants of X and Au. To compare and differentiate the ensemble and ligand effects, different numbers of Au(111) sublayers were replaced by X(111), while the lattice constant of the slab was kept fixed. The ordered alloys considered in our calculations are shown in Fig. 2. The coordinates of our computational models can be found in the supplementary material.

Random alloy (111) surfaces were modeled as a 4 layer, (3 × 3) unit cell, with the bottom two atomic layers fixed in bulk positions. A vacuum gap of at least 12 Å in the z-direction was used to separate periodic images. For each composition, more than fifteen randomly alloyed configurations were generated. Each configuration was generated by randomly mixing the two elements. Following Vegard's law,[38] the weighted average of the lattice constants between Au and X was used as the lattice constant of the slab. Randomly alloyed nanoclusters were modeled as truncated octahedra with 140 atoms (Fig. S1 of the supplementary material).[17] For each composition, at least five randomly alloyed clusters were generated. Additional information about this approach can be found in Ref. 17. A vacuum gap of at least 10 Å separated the periodic images. The clusters are denoted as X_xAu_{1-x} [where X = {Pd, Rh, Pt} and x (x = 0.25, 0.50, and 0.75) is the fraction of element X]. To calculate the average binding energies of H and O, ten triatomic ensembles were randomly sampled for each binding site.

III. RESULTS AND DISCUSSION

A. Ensemble vs. strain effects

To directly compare the ensemble and strain effects on alloyed surfaces, H- and O-binding energies were calculated on the ordered alloy surfaces with varying lattice constants from that of X (X = Pd, Rh, and Pt) to Au (4.08 Å) (Fig. 3). To ensure that the electronic contribution from the sublayers were controlled, all three sublayers were kept as Au(111). For PdAu/Au(111) and PtAu/Au(111), five lattice constants between Pd/Pt and Au were considered. Since the slab with
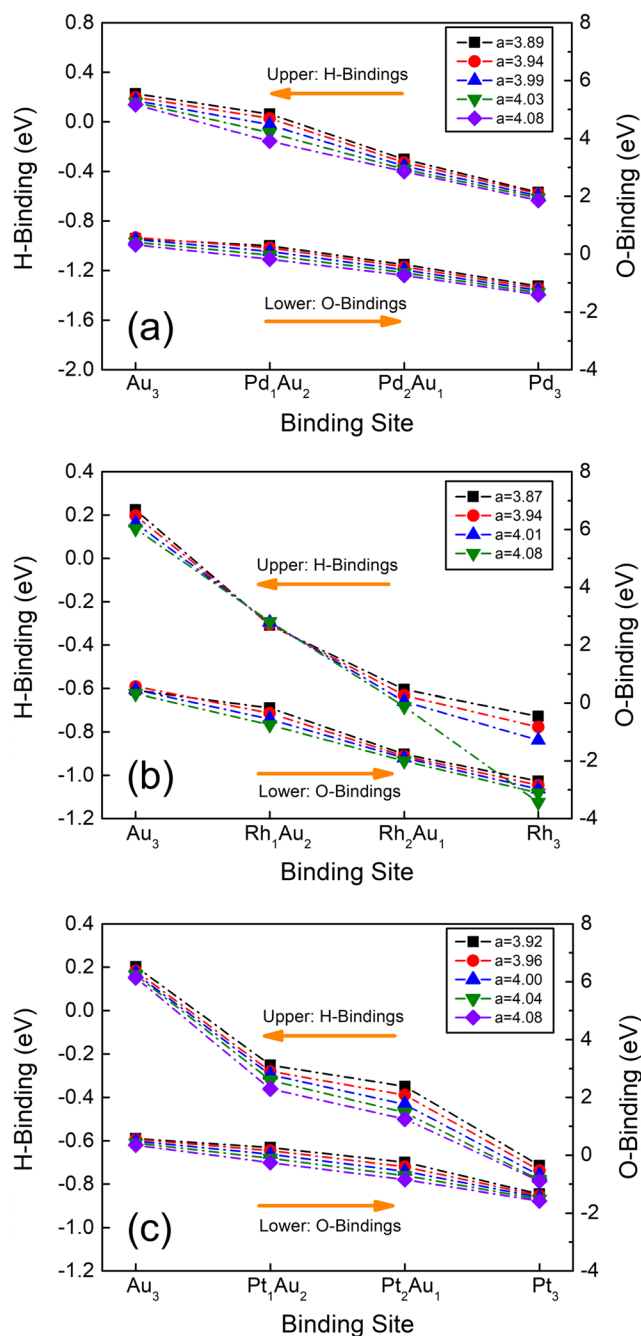

FIG. 3. Calculated H- and O-bindings at ordered alloy surfaces with varying lattice constant, a (in units of Å). H- and O-binding energies at (a) PdAu/Au(111), (b) RhAu/Au(111), and (c) PtAu/Au(111). The black, red, blue, green, and purple symbols represent the surfaces with varying lattice constants from that of X (X = Pd, Rh, and Pt) to Au (4.08 Å).

the lattice constant of Rh (3.80 Å) leads to significant surface distortion upon adsorbate binding, this smallest lattice constant was excluded from our analysis. Our calculations show that with an increase of the X component (X = Pd, Rh, and Pt) in the triatomic ensemble, both the H- and O-binding energies increase nearly linearly. With an increase in the lattice constant, both H- and O-binding energies are strengthened at the same binding site, due to the strain effect.[12,13] An exception is the Rh_1Au_2 triatomic ensemble, which has a similar H binding with varying lattice constant [Fig. 3(b)]. This can be understood from the optimized adsorption geometries shown in Fig. 4, where both H and O bind to the 3-fold hollow or (near) bridge sites of the triatomic ensemble, with the exception of the Pt_1Au_2 and Rh_1Au_2 ensembles where H optimizes to the Rh/Pt atop site. We recently reported that IrAg[33] alloys have similar H binding trends. Interestingly, for H adsorption at the ensembles of Pt_1Au_2, there was no local minimum found at the 3-fold hollow or bridge site. Since the favorable site is determined by the specific composition of the triatomic ensemble, we attribute this binding geometry to the ensemble effect.

Compared to the binding energies at different ensembles in the same bimetallic alloy, the effect of strain is less significant for tuning the H- and O-binding energies. However, if the increase in the lattice constant is relatively large, a significant tuning of the binding at the same binding site is expected. For example, with a lattice constant of 4.08 Å for PdAu/Au(111), the H binding at the ensemble of Pd_1Au_2 is close to a Pd_2Au_1 ensemble with the lattice constant of 3.89 Å [Fig. 3(a)]. If the strain is too large, an adsorption-induced relaxation could also lead to the strengthened binding, as in the case of H-binding to the highly strained Rh_3 ensemble [Fig. 3(b)].

Nevertheless, the trends of the adsorbate tunability do not change with the lattice constant, as shown in Fig. 3.

B. Ensemble vs. ligand effects

To directly compare the ensemble and ligand effects on alloyed surfaces, H- and O-binding energies were calculated on different XAu/Au(111) surfaces with varying numbers of substituted sublayers from Au(111) to X(111) (Fig. 5). To control the strain effect, the lattice constant of all slabs was kept as 4.08 Å. Interestingly, with an increase in substituted sublayers, both the H- and O-binding energies are similar. Exceptions include the ensembles of Rh_2Au_1 and Rh_3, which have significantly weakened H- and O-bindings with the increase in Rh(111) in the sublayers [Fig. 5(b)]. For PtAu/Au(111), it can be seen that the Pt_3 ensemble has also weakened H-binding upon substitution of Pt(111) sublayers, with the resulting H-binding energies close to those of Pt_1Au_2 and Pt_2Au_1 [Fig. 5(c)]. In contrast, the trends in O-binding at PtAu/Au(111) are nearly-linear [Fig. 5(c)]. This difference in the tuning of H- and O-binding energies shows that PtAu is a special bimetallic that is untunable for H but tunable for O,[6,17] breaking a well-known adsorption scaling relationship. This result has been verified in a recent collaborative theoretical and electrochemical study.[17]

Although the electronic contribution from sublayers to the surface can help tuning the H- and O-bindings on these three bimetallics, it is clear from Fig. 5 that this ligand effect is not as significant as the ensemble effect. This result is consistent with the conclusions from Liu and Nørskov,[10] where O, N, and CO adsorption on the PdAu surface depend primarily on the local adsorption environment provided by the specific atomic ensemble. It should be noted that although the strain and ligand effects only modestly change the binding energies of H and O, they can still be important for catalyst design. For example, a Pt_3 ensemble on Pt(111) is understood to possess excellent oxygen reduction reaction (ORR) performance with the O-binding only slightly stronger than the optimal, as shown in the famous ORR volcano activity plot in Ref. 39. It is expected that with some modest changes in surface electronic and/or strain, the O-binding of such a Pt_3 site could be slightly weakened, leading to even higher ORR performance.[18] In a recent study, we calculated that a Pt_3 site on Au(111) could lead to such an improvement for ORR.[6] For catalytic reactions like the ORR, many of the close-packed transition metal surface binds adsorbates very strongly (e.g., Pd, Rh, Pt, Ni, and Ir[8,17,39]), while the noble metals bind adsorbates very weakly to be active (e.g., Au and Ag[6]). Compared to the strain and ligand effects, the
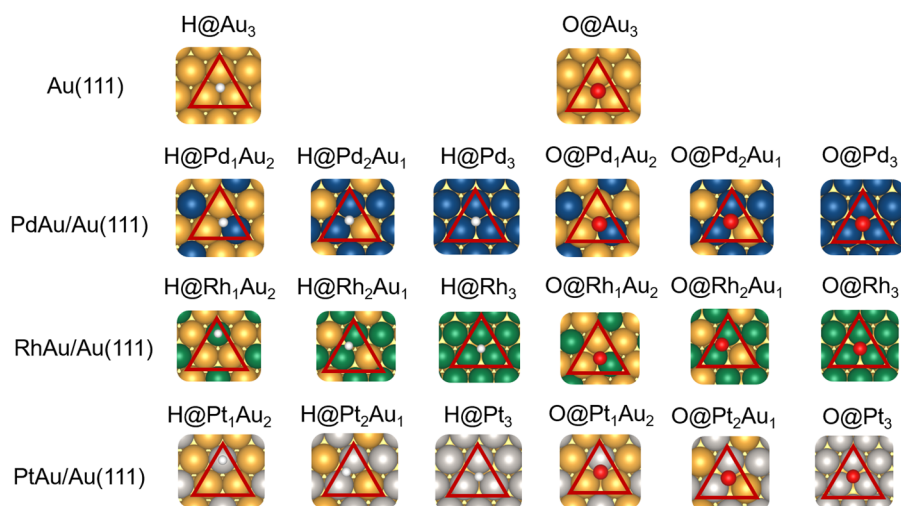

FIG. 4. H and O adsorption configurations at the triatomic ensembles of XAu/Au(111) (X = Pd, Rh, and Pt) ordered alloy slabs. White, red, gold, blue, green, and silver represent H, O, Au, Pd, Rh, and Pt, respectively.
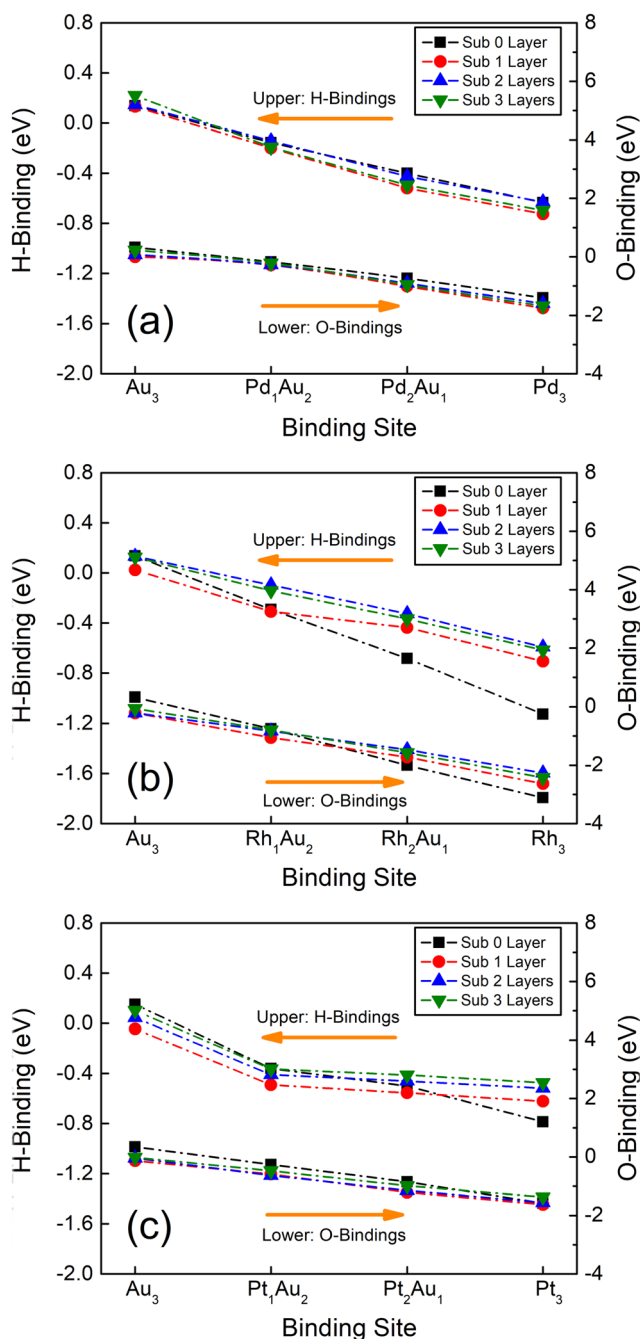
FIG. 5. Calculated H- and O-bindings at ordered alloy surfaces with varying numbers of substituted sublayers. H- and O-binding energies on (a) PdAu/Au(111), (b) RhAu/Au(111), and (c) PtAu/Au(111) surfaces. The black/gray points represent the slab without sublayer substitution. Red/pink, blue/dark cyan, and green/cyan points represent the substitution of the first 1, 2, and 3 sublayers with X(111), where X = Pd, Rh, and Pt.

ensemble effect is more important for alloys of these metals, as a way of providing a well-tuned specific ensemble that can bind adsorbates with an intermediate strength, resulting in a catalyst close to the peak of the reaction volcano.[17] An ensemble-based strategy for rational alloy catalyst design can be found in Ref. 6, where it was found that although Rh and Au are both inactive for ORR, the Rh-Au interface (more specifically, the Rh_1Au_2 ensemble) provides excellent ORR activity in RhAu alloy nanoparticles.
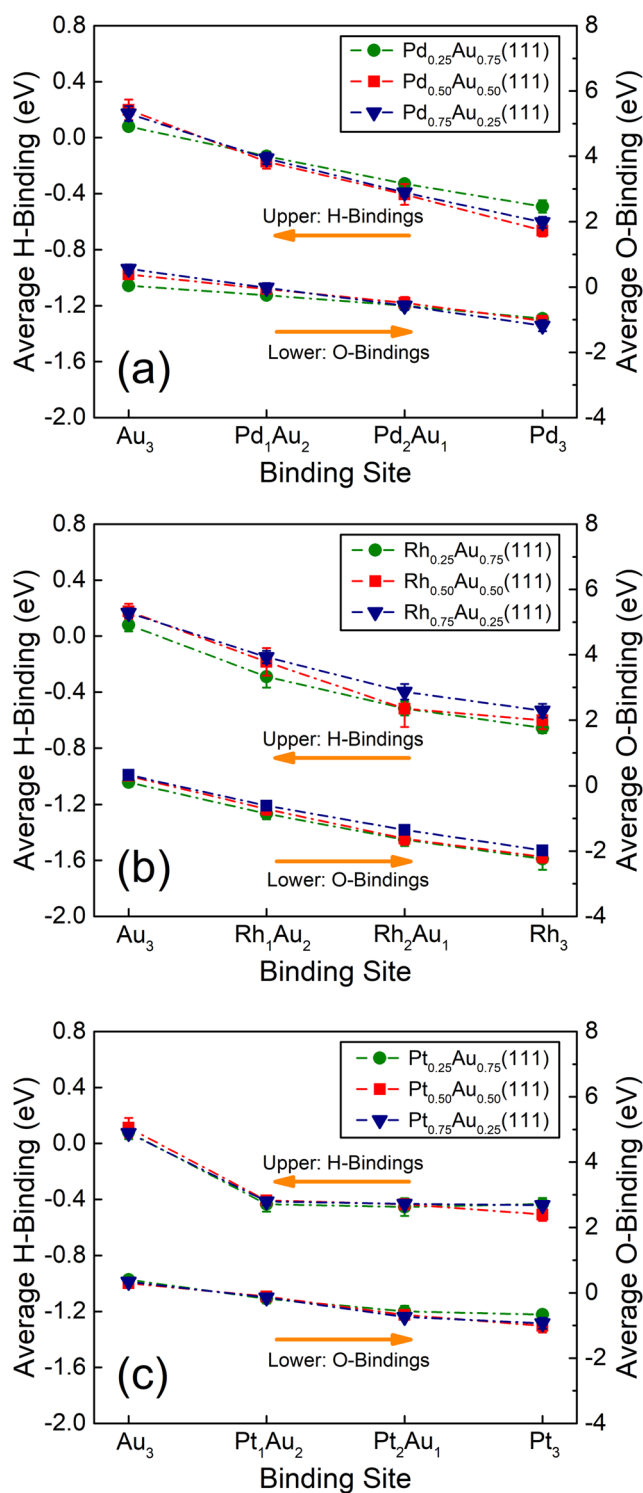

FIG. 6. Calculated H- and O-bindings at random alloy (111) slabs. [(a)–(c)] Average H- and O-binding energies at (a) $Pd_xAu_{1-x}(111)$, (b) $Rh_xAu_{1-x}(111)$, and (c) $Pt_xAu_{1-x}(111)$. Error bars indicate the standard deviation of binding energies calculated from ten sampled binding sites.

C. Random alloys

1. Random alloy slabs

From the ordered alloy surfaces, it was found that while the strain and ligand effects are able to tune the H- and O-binding energies, the ensemble effect is more significant. Since many state-of-the-art alloy synthesis methods (e.g.,

microwave-assisted synthesis[40]) are kinetically controlled, there are likely many different meta-stable alloy configurations that can be synthesized under the same conditions.[6] Therefore, variations of binding energies due to the three effects should be quantified and a model that evaluates these three effects together should be developed.

Here, to evaluate the uncertainties on the alloying effects, we calculated the average H- and O-binding energy of each binding site sampled from randomly alloyed models. Error bars indicate the standard deviations of the binding energy at the same binding site for the different sampled atomistic environments. For each alloy composition, a weighted average of the lattice constants of the two elements was used as the lattice constant, based on Vegard's law.[38] This random alloy model guarantees that all the three alloying effects are considered in the same calculation, together with error bars that evaluate the uncertainties in different randomly alloyed geometries. Figure 6 shows the average H- and O-bindings on $X_xAu_{1-x}(111)$ (X = Pd, Rh, and Pt; x = 0.25, 0.50, and 0.75) sampled from fifteen random geometries. It can be clearly seen that $Pd_xAu_{1-x}(111)$ tunes H-bindings linearly with the increase in Pd in a triatomic ensemble [Fig. 6(a)], while $Rh_xAu_{1-x}(111)$ is less linear [Fig. 6(b)] and $Pt_xAu_{1-x}(111)$ is almost untunable among different Pt-related triatomic ensembles [Fig. 6(c)]. These calculations show differences in H tunability in the following three bimetallics: PdAu > RhAu > PtAu. However, for O adsorption, the binding energies of all these three bimetallics tune near-linearly, indicating good O tunability with the increase in Pd/Rh/Pt atoms in the triatomic ensemble. The differences in the binding energies at different alloy compositions are also less significant than the ensemble effect, showing less influence from the strain and ligand effects, in good agreement with the conclusions drawn from the ordered alloy surfaces. Also, the error bars are relatively small, indicating that the binding energies and their tunabilities depend primarily on the atomic ensemble, while variation of H- and O-bindings is less significant with different random geometries.

Figure 7 shows the representative H- and O-binding configurations on random alloy surfaces. It is found that the H- and O-binding sites are similar to those on the ordered alloys shown in Fig. 4, with the exception that H prefers to stay at the three-fold hollow site on Rh_1Au_2 instead of the Rh atop site.

So while the results from the random alloy and the ordered alloy surfaces are similar, there are minor differences in both the binding energies and sites which may be important for a quantitative description of adsorbate binding.

2. Random alloy clusters

The ligand, strain, and ensemble effects were also considered on a 140-atom cluster model of a 2 nm nanoparticle (Fig. 8). Our previous studies have shown that a cluster model has better agreement with experiments of small nanoparticles, as compared to slab models.[18] Compared to the random slab model in Fig. 6, the trends in the average H- and O-bindings are generally similar to the cluster, while the error bars of the cluster models are slightly larger (Fig. 8). This is because some binding sites were near the edge and corner of the cluster, which have stronger binding due to lower surface coordination as compared to the (111) surface in the slab model. The adsorption geometries of H and O at cluster surfaces are also similar to those at the slab (Fig. 7). Therefore, we conclude that on both cluster and slab models of random alloys, tuning of adsorbate binding is primarily affected by the atomic ensemble and less by strain and electronic interactions.

To test the generality of our results, we selected six more bimetallic alloys that include a "strong binding metal" (Pd, Rh, and Pt) and a "weak binding metal" (Ag and Cu), with the 140-atom random alloy cluster model (Fig. 9). With the conclusions from Figs. 6 and 8 showing that the composition does not lead to significant changes in the H- and O-binding energy trends, we considered only a 0.50:0.50 alloy composition here. It can be seen from the results that $Pd_{0.50}Ag_{0.50}$ and $Pd_{0.50}Cu_{0.50}$ have good tunability for H-binding, while $Rh_{0.50}Ag_{0.50}$, $Pt_{0.50}Ag_{0.50}$, $Rh_{0.50}Cu_{0.50}$, and $Pt_{0.50}Cu_{0.50}$ have a relatively weaker tunability for H-bindings at Rh- or Pt-related sites [Fig. 9(a)]. On the other hand, $Pd_{0.50}Ag_{0.50}$, $Rh_{0.50}Ag_{0.50}$, $Pd_{0.50}Cu_{0.50}$, and $Rh_{0.50}Cu_{0.50}$ have tunable O-bindings at Pd- or Rh-related sites, while $Pt_{0.50}Ag_{0.50}$ and $Pt_{0.50}Cu_{0.50}$ have weaker tunability of O-binding at Pt-related sites [Fig. 9(b)]. Interestingly, since Cu binds to H weaker but binds to O stronger than Pd and Pt, both $Pd_{0.50}Cu_{0.50}$ and $Pt_{0.50}Cu_{0.50}$ have inverted tuning trends of H and O adsorptions: with the increase in the Pd or Pt component in the triatomic ensemble, H binding becomes stronger while O binding
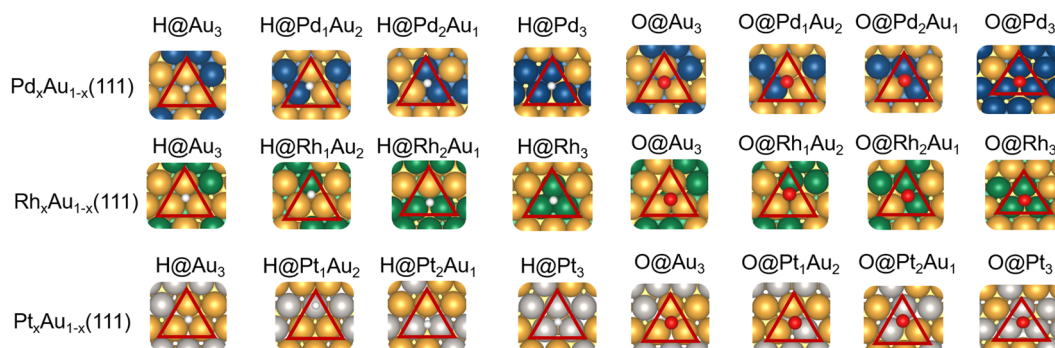

FIG. 7. Selected typical H and O adsorption configurations at the triatomic ensembles of $X_xAu_{1-x}(111)$ (X = Pd, Rh, and Pt) random alloy slabs. White, red, gold, blue, green, and silver represent H, O, Au, Pd, Rh, and Pt, respectively.
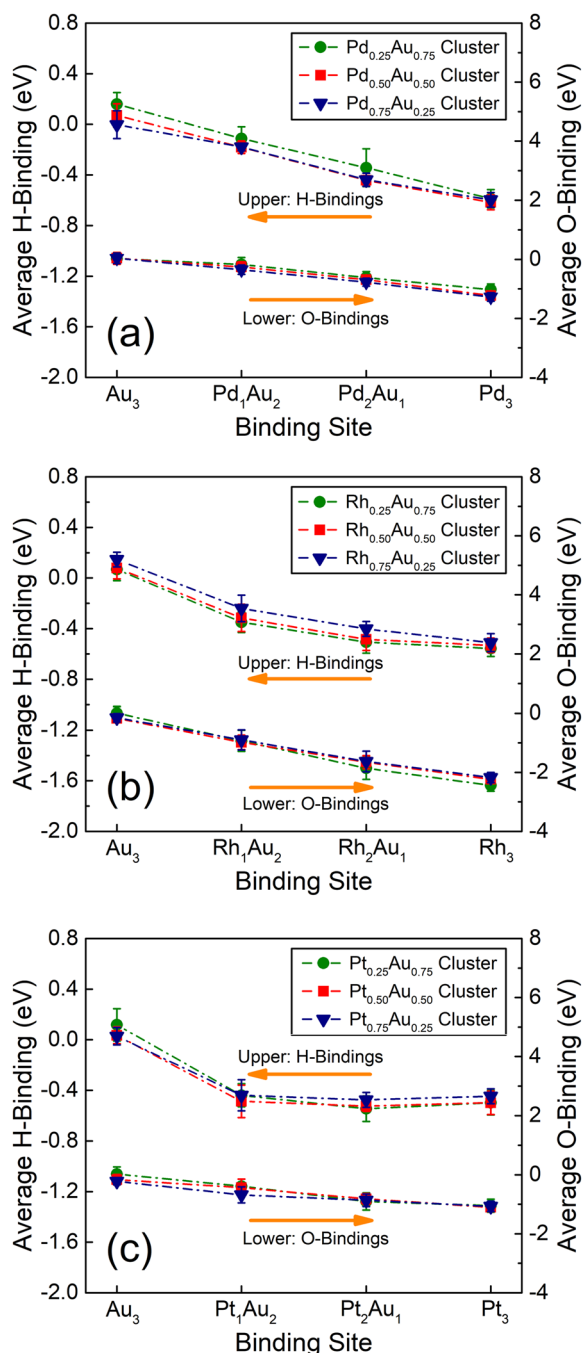
FIG. 8. Calculated H- and O-binding energies on random alloy 140-atom clusters. Average H- and O-bindings at (a) Pd_xAu_{1-x}, (b) Rh_xAu_{1-x}, and (c) Pt_xAu_{1-x}. All binding sites were sampled from the (111) facets of the clusters. Error bars show the standard deviation of the binding energies calculated from ten sampled binding sites.

FIG. 9. Calculated averaged (a) H- and (b) O-binding energies of $Pd_{0.50}Ag_{0.50}$, $Rh_{0.50}Ag_{0.50}$, $Pt_{0.50}Ag_{0.50}$, $Pd_{0.50}Cu_{0.50}$, $Rh_{0.50}Cu_{0.50}$, and $Pt_{0.50}Cu_{0.50}$. All binding sites were sampled from the (111) faces of the clusters. Error bars indicate the standard deviation of binding energies calculated from ten sampled binding sites.

elements, such as differences in their lattice constants, electronic charge transfer between them, and adsorbate-induced relaxation. Electronic and/or strain effects can have non-negligible contributions to the binding energy for these alloys, raising the uncertainty in adsorbate binding energies.

IV. CONCLUSIONS

In this paper, we have explored the ensemble, ligand, and strain effects of close-packed surfaces alloyed by the transition metals with strong and weak H- and O-binding energies. PdAu, RhAu, and PtAu were selected as typical bimetallics, and both ordered and random alloy surfaces were studied to compare the tunability of H- and O-binding energies as a function of the lattice constant, numbers of alloyed sublayers, and random alloy geometries. We found that when alloying two elements with strong and weak adsorption capacities, the ensemble effect more significantly tunes the adsorbate binding than the ligand and strain effects. Similar conclusions were found for a range of other bimetallics, but also that minor changes in adsorbate bindings, due to the ligand and strain effects, cannot be neglected in a quantitative model. It is expected that for bimetallics with alloys of two strong adsorption elements (e.g., PdPt[45] and RhPd[32]), the ligand and strain will be more important.

becomes weaker. We expect that these reverse trends, which are due to the special oxophilic properties of Cu, could be beneficial to bi-functional alloy catalyst design. Specifically, for CO oxidation, it is found that many transition metals suffer from CO poisoning, while alloying those elements with Cu can promote oxygen adsorption and CO oxidation.[41–44] Additionally, it should be mentioned that compared to the Au-based alloys shown in Fig. 8, some Ag- and Cu-based alloys have relatively large distributions of H- and O-binding energies (Fig. 9), which could originate from intrinsic differences between the two
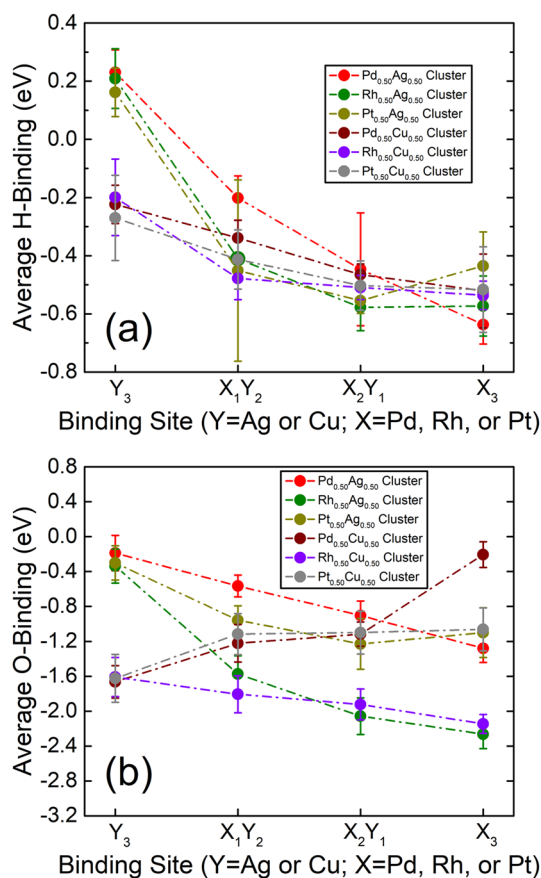
SUPPLEMENTARY MATERIAL

See supplementary material for the geometry of 140-atom cluster and coordinates of ordered alloy surfaces.

[1] L. Zhang, R. M. Anderson, R. M. Crooks, and G. Henkelman, Surf. Sci. **640**, 65 (2015).

[2] R. M. Anderson, D. F. Yancey, L. Zhang, S. T. Chill, G. Henkelman, and R. M. Crooks, Acc. Chem. Res. **48**, 1351 (2015).

[3] A. K. Sharma and B. D. Gupta, Nanotechnology **17**, 124 (2006).

[4] L. Schlapbach and A. Züttel, Nature **414**, 353 (2001).

[5] Y. Yao, Z. Huang, P. Xie, S. D. Lacey, R. J. Jacob, H. Xie, F. Chen, A. Nie, T. Pu, M. Rehwoldt, D. Yu, M. R. Zachariah, C. Wang, R. Shahbazian-Yassar, J. Li, and L. Hu, Science **359**, 1489 (2018).

[6] H. Li, L. Luo, P. Kunal, C. S. Bonifacio, Z. Duan, J. C. Yang, S. M. Humphrey, R. M. Crooks, and G. Henkelman, J. Phys. Chem. C **122**, 2712 (2018).

[7] H. Li and G. Henkelman, J. Phys. Chem. C **121**, 27504 (2017).

[8] P. Kunal, H. Li, B. L. Dewing, L. Zhang, K. Jarvis, G. Henkelman, and S. M. Humphrey, ACS Catal. **6**, 4882 (2016).

[9] S. García, L. Zhang, G. W. Piburn, G. Henkelman, and S. M. Humphrey, ACS Nano **8**, 11512 (2014).

[10] P. Liu and J. K. Nørskov, Phys. Chem. Chem. Phys. **3**, 3814 (2001).

[11] N. Takehiro, P. Liu, A. Bergbreiter, J. K. Nørskov, and R. J. Behm, Phys. Chem. Chem. Phys. **16**, 23930 (2014).

[12] M. Mavrikakis, B. Hammer, and J. Nørskov, Phys. Rev. Lett. **81**, 2819 (1998).

[13] L. Zhang and G. Henkelman, J. Phys. Chem. C **116**, 20860 (2012).

[14] K. W. Park, J. H. Choi, B. K. Kwon, S. A. Lee, Y. E. Sung, H. Y. Ha, S. A. Hong, H. Kim, and A. Wieckowski, J. Phys. Chem. B **106**, 1869 (2002).

[15] D. A. Slanac, W. G. Hardin, K. P. Johnston, and K. J. Stevenson, J. Am. Chem. Soc. **134**, 9812 (2012).

[16] W. Y. Yu, G. M. Mullen, D. W. Flaherty, and C. B. Mullins, J. Am. Chem. Soc. **136**, 11070 (2014).

[17] L. Luo, Z. Duan, H. Li, J. Kim, G. Henkelman, and R. M. Crooks, J. Am. Chem. Soc. **139**, 5538 (2017).

[18] L. Zhang, R. Iyyamperumal, D. F. Yancey, R. M. Crooks, and G. Henkelman, ACS Nano **7**, 9168 (2013).

[19] R. Si, J. Liu, K. Yang, X. Chen, W. Dai, and X. Fu, J. Catal. **311**, 71 (2014).

[20] G. E. Gdowski, T. E. Felter, and R. H. Stulen, Surf. Sci. **181**, L147 (1987).

[21] M. Pan, D. W. Flaherty, and C. B. Mullins, J. Phys. Chem. Lett. **2**, 1363 (2011).

[22] E. J. Evans, H. Li, W. Y. Yu, G. M. Mullen, G. Henkelman, and C. B. Mullins, Phys. Chem. Chem. Phys. **19**, 30578 (2017).

[23] W.-Y. Yu, L. Zhang, G. M. Mullen, G. Henkelman, and C. B. Mullins, J. Phys. Chem. C **119**, 11754 (2015).

[24] W. Y. Yu, G. M. Mullen, and C. B. Mullins, J. Phys. Chem. C **117**, 19535 (2013).

[25] W. Y. Yu, G. M. Mullen, and C. B. Mullins, J. Phys. Chem. C **118**, 2129 (2014).

[26] H. Li, E. J. Evans, C. B. Mullins, and G. Henkelman, J. Phys. Chem. C **122**, 22024 (2018).

[27] D. W. Yuan and Z. R. Liu, J. Power Sources **224**, 241 (2013).

[28] G. Binnig and H. Rohrer, Surf. Sci. **126**, 236 (1982).

[29] T. Bligaard, J. K. Nørskov, S. Dahl, J. Matthiesen, C. H. Christensen, and J. Sehested, J. Catal. **224**, 206 (2004).

[30] G. Jones, T. Bligaard, F. Abild-Pedersen, and J. K. Nørskov, J. Phys.: Condens. Matter **20**, 064239 (2008).

[31] S. Seraj, P. Kunal, H. Li, G. Henkelman, S. M. Humphrey, and C. J. Werth, ACS Catal. **7**, 3268 (2017).

[32] G. W. Piburn, H. Li, P. Kunal, G. Henkelman, and S. M. Humphrey, ChemCatChem **10**, 329 (2018).

[33] H. Guo, H. Li, K. Jarvis, H. Wan, P. Kunal, S. Dunning, Y. Liu, G. Henkelman, and S. Humphrey, "Microwave-assisted synthesis of classically immiscible Ag-Ir alloy nanoparticle catalysts," ACS Catal. (to be published).

[34] J. P. Perdew, K. Burke, and M. Ernzerhof, Phys. Rev. Lett. **77**, 3865 (1996).

[35] P. E. Blöchl, Phys. Rev. B **50**, 17953 (1994).

[36] W. Kohn and L. J. Sham, Phys. Rev. **140**, A1133 (1965).

[37] H. Monkhorst and J. Pack, Phys. Rev. B **13**, 5188 (1976).

[38] A. R. Denton and N. W. Ashcroft, Phys. Rev. A **43**, 3161 (1991).

[39] J. K. Nørskov, J. Rossmeisl, A. Logadottir, L. Lindqvist, J. R. Kitchin, T. Bligaard, and H. Jónsson, J. Phys. Chem. B **108**, 17886 (2004).

[40] N. Dahal, S. García, J. Zhou, and S. M. Humphrey, ACS Nano **6**, 9433 (2012).

[41] Y. Liu, H. Li, W. Cen, J. Li, Z. Wang, and G. Henkelman, Phys. Chem. Chem. Phys. **20**, 7508 (2018).

[42] L. Zhang, H. Y. Kim, and G. Henkelman, J. Phys. Chem. Lett. **4**, 2943 (2013).

[43] K. Shin, L. Zhang, H. An, H. Ha, M. Yoo, H. M. Lee, G. Henkelman, and H. Y. Kim, Nanoscale **9**, 5244 (2017).

[44] B. Liu, Z. Zhao, G. Henkelman, and W. Song, J. Phys. Chem. C **120**, 5557 (2016).

[45] C. Y. Lu and G. Henkelman, J. Phys. Chem. Lett. **2**, 1237 (2011).